Typical MIMO propagation channels in urban macrocells at 2GHz

Jean-Marc Conrat, Patrice Pajusco

Typical MIMO propagation channels in urban macrocells at 2 GHz

Jean-Marc Conrat, Patrice Pajusco
France Télécom R&D, 6, av. des Usines, BP 382 - 90007 Belfort Cedex, France
E-mail: jeanmarc.conrat@orange-ftgroup.com, patrice.pajusco@orange-ftgroup.com

***Abstract* — A directional wideband measurement campaign was performed in urban macrocells at 2 GHz using a channel sounder and a 8-sensor linear antenna array at the base station. Directions of arrival at the Base Station (BS) were estimated by beamforming using the antenna array. Directions of arrival at the Mobile Station (MS) were estimated by beamforming using parts of the measurement route. Global parameters (delay spread, azimuth spread at BS, maximum factor and street canyon factor) were processed from the Azimuth-Delay Power Profiles (ADPP) at BS and MS. In this paper, we compare the statistics of these four parameters with the statistics of those simulated by the 3GPP-SCM system-level model and the statistics of those reported in the literature. We find an acceptable agreement between our measurements and the SCM model except for the delay spread and the street canyon factor. The azimuth spread at BS mean value (9.5°) and delay spread mean value (0.250 µs) are also in accordance with values reported in other references. Azimuth spreads are ranged from 7° to 11°, and delay spreads are ranged from 0.1 µs to 1 µs. From a statistical analysis of global parameters, we show that most of the measured propagation channels can be classified in three main categories: low spatial diversity at MS and BS, high spatial diversity at MS and BS, low spatial diversity at BS and high spatial diversity at MS.**

I. INTRODUCTION

Multiple antenna radio access (MIMO) based on antenna arrays at both the Mobile Station (MS) and the Base Station (BS) has recently emerged as a key technology in wireless communication, increasing the data rates and system performance [1, 2]. This technique exploits both the spatial and polarization diversities of multipath channels in rich scattering environments. The benefits of multiple antenna technologies can be shown by achieving link-level or system-level simulations. Both studies require a realistic MIMO propagation channel model.

There are two principal MIMO propagation channel types [3, 4]: physical and non-physical models. Non-physical models are based on the statistical description of the channel using non-physical parameters, such as the signal correlation between the different antenna elements at the receiver and transmitter [5, 6]. In contrast, physical models provide either the location and electromagnetic properties of scatterers or the physical description of rays. A ray is described by its delay, Direction of Arrival (DoA), Direction of Departure (DoD) and polarization matrix. Geometrical models [7-9], directional tap models [10, 11] or ray tracing [12, 13] are examples of physical models. Both approaches have advantages and disadvantages but physical models seem to be more suitable for MIMO applications because they are independent of the antenna array configuration [14, 15]. Furthermore, they inherently preserve the joint properties of the propagation channel in temporal, spatial and frequential domains. By taking into account antenna diagrams, Doppler spectrum or correlation matrices can be coherently deduced from a physical model.

For outdoor wide area scenarios, the most commonly used physical MIMO propagation channel is the 3GPP/3GPP2 SCM model [16]. In the SCM system-level model, most parameters are defined by their probability density functions. This randomized approach gives a very realistic description of the propagation channel in the sense that it provides a very large variety of channels. However, the use of a randomized model in link-level simulations implies a great number of simulations in order to comply with the probability density function of randomized parameters. In the case of accurate link-level simulation, it leads to an enormous simulation time. More recently, the 3GPP have defined new models based on tapped delay-line models with fixed values for angular parameters or correlation matrices. These models simplify link-level simulations and reduce the amount of simulation time but on the other hand, the great variability of MIMO propagation channels is not taken into account. For instance, [17] defines only two profiles in urban macrocell environment.

The scope of this paper is to investigate an intermediate modeling approach between the full randomized approach and the single profile approach. The basic idea is to define a limited number of channels with fixed values for power, delays and angular parameters, and for each channel to give a percentage of occurrences. The definition of these channels is performed in four steps:

1- Measurement campaign and physical parameter estimation. (part 2)
2- Global parameter processing: global parameters are an extension of the traditional synthetic parameters used in wideband analysis. They represent all possible metrics that characterize the propagation channel, for example the delay spread, the azimuth spread, the number of paths, the Rice factor, etc. A similar concept can be found in the SCM model that defines the azimuth spread, delay spread and shadowing factor as "bulk parameters". Part 3 describes the different global parameters that were used, gives their Probability Density Function (PDF) and compares

them to the PDF given by the SCM model when possible.

3- Group detection (part 4): during this step, measured channels fall into groups, where the global parameters of channels in the same group are similar and the global parameters of channels in different groups are dissimilar. In the field of statistics, this is called clustering analysis. In this paper, we prefer to use the term group instead of cluster to avoid the confusion with the cluster defined in geometrical models.
4- Typical case selection: A typical case for a given channels group corresponds to a measured channel whose global parameters are close to the median global parameters of the given channels group. A typical case is then considered as a model and the physical parameters estimated in step 1 can be used in link-level or system-level simulation. [18] describes a channel simulator that processes the impulse response (or impulse responses matrix in the case of MIMO simulation) from the physical parameters of a set of rays.

Finally to complete the typical case analysis and the statistical analysis of global parameters, part 5 comments on the correlation between the global parameters.

II. Measurement Campaign and Data Processing

The measurement scenario emulated an up-link, the transmitter of a propagation channel sounder being the mobile and the receiver the base station (fig. 1). The carrier frequency was 2.2 GHz and the analyzed bandwidth 10 MHz. A standard vertical dipole antenna was used at the transmitter and was located on the roof of a car. An antenna array made up of 10 vertical sectorial sensors regularly spaced (5 cm = 0.36 λ) was used at BS. The array antenna was set up on the rooftop of 3 buildings and oriented in 3 directions for each building. One snapshot was a simultaneous measurement of 10 complex impulse responses (CIRs). A measurement route consisted of 600 snapshots triggered in time. The mobile terminal vehicle was driven at a predetermined speed such that the snapshots were collected each λ/3. The measurement was conducted in urban and dense urban macrocells. The main difference between the two environments is the building height. In urban macrocells (Mulhouse, east of France), the average height is approximately 20 meters, in dense urban macrocells (Paris), the average height is approximately 30 meters. Further details about the measurement setup and the previous propagation analysis can be found in [19-21].

The measurement route was divided into sections containing 50 snapshots and consecutive sections were shifted by the section size. A section defines a virtual linear antenna array at the mobile and can be considered as a 10*50 MIMO measurement point. A total amount of 804 MIMO points was selected for this study. The distance BS-MS (*Dist*) ranges between 0 m and 750 m (fig. 3). The mobile azimuth (*MS-Azi*) is roughly uniformly distributed between 0° and 90° (fig. 4). *MS-azi* is the difference between the mobile motion azimuth and the BS-MS azimuth. It ranges between 0° and 90 °. 0° indicates a car trajectory parallel to the line BS-MS. 90° indicates a car trajectory perpendicular to the line BS–MS.

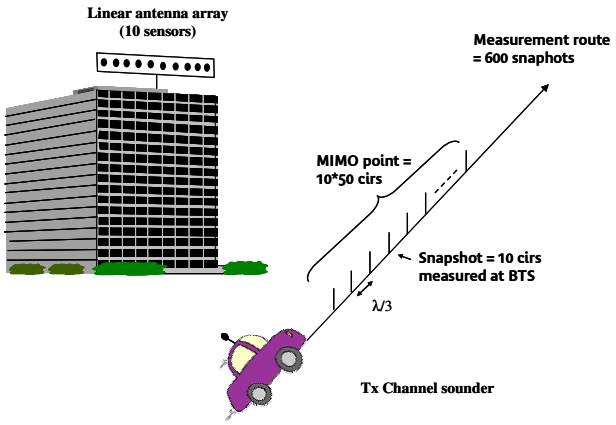

Figure 1: Measurement campaign description

Azimuth Power Delay Profile (*ADPP)* at BS and MS were estimated by a Bartlett beamforming method. Such an approach is fast and very convenient for analyzing a large collection of data. Examples of space-time diagrams are given in figures 14-19. Rays with a zero BS-azimuth are in the perpendicular direction to the BS antenna array. Rays with an MS-azimuth equal to -180° or 0° are in the direction of the car motion, 0° being the front direction, -180° being the back direction. The vertical dark line indicates the BS-MS direction.

From an extended visual inspection of $ADPP_{MS}(\tau,\phi)$ and $ADPP_{BS}(\tau,\phi)$, some preliminary conclusions can be drawn: The propagation channel is clustered at BS and MS, i.e. $ADPP_{MS}(\tau,\phi)$ and $ADPP_{BS}(\tau,\phi)$ show local areas centered around an azimuth and a delay where the power is concentrated. Delays, azimuths and powers of clusters were estimated by local maximum detection on $ADPP_{BS}(\tau,\phi)$ and $ADPP_{MS}(\tau,\phi)$. Due to the limited angular and temporal resolution of the estimation method, the intra-cluster characteristics were not investigated in this paper. A more detailed description of this method can be found in [21]. We define a mobile cluster (MS-cluster) as a local maximum of $ADPP_{MS}(\tau,\phi)$ and note $P_{MS\text{-}cluster}(i)$ and $\phi_{MS\text{-}cluster}(i)$ the power and azimuth of the *ith* MS-cluster.

A significant drawback of the data processing is the conical ambiguity for the MS-DoA estimation. If we assume that rays arrive at the mobile in a horizontal plane, we cannot distinguish the right and left parts of $ADPP_{MS}(\tau,\phi)$. The right and left sides are defined compared with the mobile direction. Such an analysis can not properly characterize MS-DoAs but it is simple and provides valuable information on particular phenomena at MS. For instance, it can be used to evaluate the street canyon or dominant path effects. The street canyon effect corresponds to the situation where the received power is concentrated in the street axis. The dominant path effect

corresponds to the situation where the $ADPP_{MS}(\tau,\phi)$ is dominated by a single MS-cluster.

III. STATISTICAL ANALYSIS

A. Definition of global parameters

In this section, we present the global parameters that were used to identify typical/atypical measurement files. Global parameters were processed from delays, azimuths and powers estimated in the previous section. The key idea in the global parameters definition was to quantify the frequential diversity, the spatial diversity at BS and spatial diversity at MS. We also tried to limit the number of global parameters in order to optimize the group detection analysis. For instance, we did not keep global parameters that were redundant.

The first two global parameters are the traditional azimuth spread at BS (*AS*), and delay spread (*DS*) that characterize the spatial diversity at BS and the frequential diversity. At MS, no azimuth spread can be processed due to the conical ambiguity in the azimuth estimation. Two alternative parameters that represent as realistically as possible the spatial diversity at MS were defined. The first one is the maximum factor (*MaxF*) defined by (1):

$$MaxF = \frac{\max_i \left(P_{MS-Cluster}(i)\right)}{\sum_i \left(P_{MS-cluster}(i)\right)} \quad (1)$$

A maximum factor close to 0 tends to indicate a uniform distribution of the power around the mobile and thus a high potential spatial selectivity at MS. A maximum factor close to one indicates a quasi-LoS situation and thus a low potential spatial diversity at MS. The second one is the street canyon factor (*ScF*) defined by (2). The street canyon area is defined by figure 2.

$$ScF = \frac{\sum_{\{i|\phi(i) \text{ inside sc area}\}} \left(P_{MS\text{-}cluster}(i)\right)}{\sum_i P_{MS\text{-}cluster}(i)} \quad (2)$$

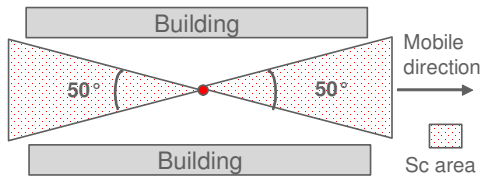

Figure 2: Sc area definition

B. Comparison of global parameters with the 3GPP-SCM

Figures 5-8 give the histograms of *DS*, *AS*, *ScF* and *MaxF*. For each figure, the equivalent histogram according to the standard SCM urban macrocell model (without any option) is given. The following conclusions can be drawn:

- SCM *AS* values are in agreement with the measured *AS* values. Measured *AS* values of about 15° were often observed in dense urban environment. *AS* values of about 8° were observed in urban environment.
- *DS* values are overestimated by the SCM macrocell model. A *DS* mean value of 0.65 µs corresponds to the atypical group HighDS described in part IV. Relative to *DS* values, our measurements are better fitted by the SCM urban micro model.
- No comparison is performed for *MaxF*, which strongly depends on the number of MS-clusters. The mean number of MS-clusters calculated from the measurement data is 20. But, the SCM model assumes 6 paths defined at MS by a mean direction and a power angular Laplacian distribution with a 35° standard deviation. A straightforward comparison would automatically lead to erroneous conclusions.
- The statistical distribution of *ScF* with the standard SCM model is shown in figure 7. If the street canyon option of SCM is selected, then, in 90% of cases, *ScF* is equal to 1 and the mean direction at MS of the 6 paths is either 0° or 180°. Compared to our measurements, the standard version of SCM underestimates *ScF* and the street canyon option overestimates it. If we consider that a mobile experiences the street canyon effect when *ScF* is higher than 0.6, then the percentage of MS that experiences a SC effect would be equal to 38%.

C. Literature review

In this paragraph, the global parameter values are compared with values reported in previous references. Table 1 sums up MISO, SIMO or MIMO measurement campaigns in urban environment that present a statistical analysis of the delay spread and azimuth spread at BS. Table 1 also contains the elevation spread at BS or MS or azimuth spread at MS when these parameters could be extracted from the measurement data. There is an acceptable agreement between our results and those listed in table 1. Nevertheless, the dispersion of the delay spread values is somewhat unexpected. It is perhaps due to the large variety of urban environments including different averaged building heights, street widths, etc. We note that there are still very few available results on the spatial properties of the propagation channel at the mobile.

Regarding *ScF* and *MaxF*, the comparison is not straightforward. Firstly, there are few references that have investigated the street canyon effect [22-25] or the dominant path effect [26] and secondly, the definition of metrics used to characterize these two propagation mechanisms are different from those given in section III-A. For example:

- [24] defines the street canyon area as being the area where the elevation at the mobile is lower than 10°. In urban macrocell environments, *ScF* is ranged between 30% and 40%.
- [26] analyses the DoAs at BS. Space-time power diagrams are compared with geographical maps by visual inspection and clusters are classified into three main classes: street-guided propagation, propagation over rooftops and scattering from high rise objects. A cluster is defined as a group of paths which have similar azimuth, elevation and delay values. [26] indicates that

the power of clusters belonging to the class "street canyon" is generally higher than 80 % of the total received power. [26] also shows that, in 90 % of cases, 55% of the total received power is concentrated in the strongest cluster. In our measurement, 55% of the power is concentrated in the strongest cluster in only 25 % of the cases. The differences between [26] and our results could be explained by the definition of the cluster concept: a cluster according to the definition of [26] may gather one or several clusters according to our definition (local maxima of $ADPP_{MS}(\tau,\phi)$).

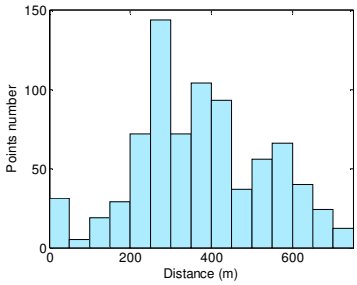

Figure 3: Histogram of *Dist*

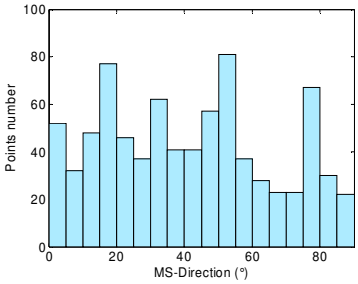

Figure 4: Histogram of *MS-Azi*

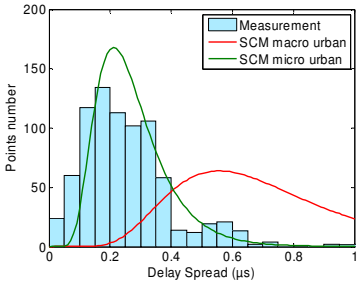

Figure 5: Histogram of *DS*

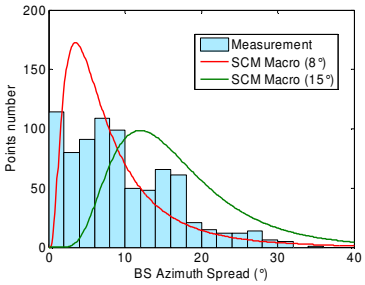

Figure 6: Histogram of *AS*

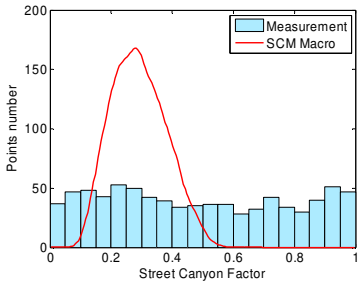

Figure 7: Histogram of *ScF*

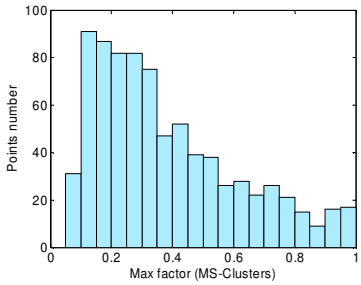

Figure 8: Histogram of *MaxF*

Location	R&D institutions	Bandwidth	Frequency	DS (µs)	BS-AS (°)	BS-ES (°)	MS-AS (°)	MS-ES (°)	Ref.
Paris Mulhouse	France Télécom R&D	10 MHz	2.2 GHz	0.25	9.5				This paper
Frankfurt	Deutsche Telekom	6 MHz	1.8 GHz	0.5	8				[27]
Norway	Telenor	50 MHz	2.1 GHz	0.056	9.9				[28]
Sweden	Telia	150 MHz	1.8 GHz	0.11	8				[29]
Sweden	Telia	150 MHz	1.8 GHz	0.075	7				[30]
Aarhus Stockholm	Uni. Aalborg	5 MHz	1.8 GHz	0.6 / 1.2	7.5 / 11				[31]
Bristol	Uni. Bristol	20 MHz	1.9 GHz	0.44	10				[32]
Bristol	Uni. Bristol	20 MHz	1.9 GHz 2.1 GHz	0.13	9				[33]
Bristol	Uni. Bristol	20 MHz	1.9 GHz 2.1 GHz	0.3			73.5		[34]
Helsinki	Uni. Helsinki	60 MHz	5.3 GHz		7.6	1.7	52.3	7.7	[35]
Helsinki	Uni. Helsinki	30 MHz	2.1 GHz	0.65 / 1.27					[23]
Munich	Uni. Illmenau	120 MHz	5.3 GHz	0.06	7		70		[36]
Stockholm	Ericsson	200 MHz	5.25 GHz	0.250	20		75	20	[37]

Table 1: Delay spread and azimuth spread comparison

IV. TYPICAL AND ATYPICAL PROPAGATION CHANNELS

To identify the different groups, a hybrid method combining hand-made filtering and K-means algorithm was used. The K-means method partitions the MIMO points into K mutually exclusive groups, such that MIMO points within each group are as close to each other as possible, and as far from MIMO points in other groups as possible. The hand-made filtering was applied to extract atypical groups and the K-means algorithm was applied to identify typical groups. The K-means algorithm gave the best results when the number of groups were equal to three and when the global parameters used in the partitioning were *DS*, *AS* and *MaxF* normalized to their standard deviation.

The partitioning proposed in this paper is a little arbitrary and alternative partitioning schemes may be found. Furthermore, the percentage of occurrences depends strongly on the measurement locations. For instance, if *Dist* was limited to 200 m, the atypical group HighDS would be mutated into a typical group. Nevertheless, the selected groups give a general and realistic overview of the various propagation channels experienced by the mobile in a macrocell environment.

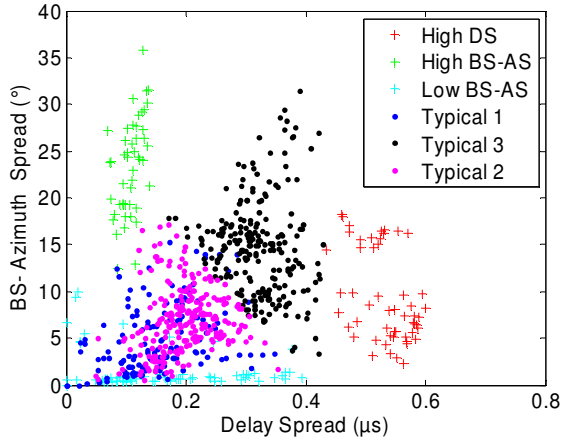

Figure 9: Selection of typical and atypical files

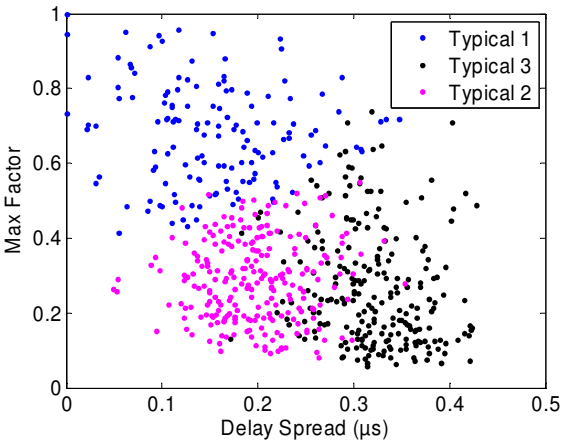

Figure 10: Selection of typical files, plot *MaxF* vs *DS*

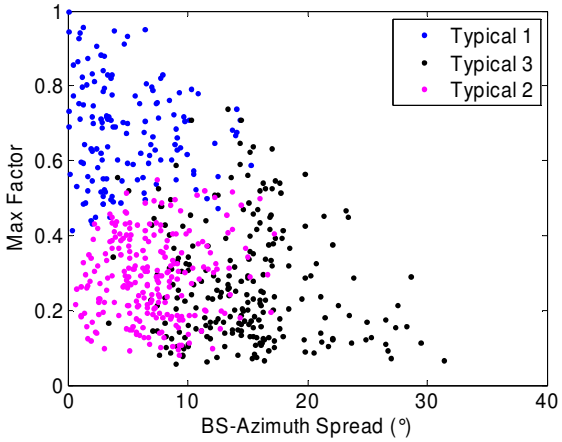

Figure 11: selection of typical files, plot *MaxF* vs *AS*

The global parameter statistics of the typical and atypical groups are summarized in table 2.

Group HighDS (fig. 17): This group gathers MIMO points with a delay spread higher than 0.4 µs. In most cases, the impulse response is divided into two discontinuous parts. The second part generally occurs at an excess delay higher than 2 µs.

Group HighAS (fig. 18): This group is more representative for a microcell environment than a macrocell environment (higher *AS*, lower *DS*). The power angular dispersion at BS created by scatterer objects in the vicinity of the BS is intensified by the short MS-DS distance (*Dist* median value =32m).

Group LowAS (fig. 19): This group was obtained by filtering measurements with *MS-Azi* smaller than 10°. In this case, we obtain a group of MIMO points with very low *AS*, and very large *MaxF* and *ScF*. It physically corresponds to scenarios where the street canyon and dominant path effects dominate the propagation conditions.

Group Typical1 (fig. 14): The vast majority of channels of this group have characteristics similar to those extracted from LOS measurements (low spatial diversity, low frequential diversity) even if there is no BS-MS visibility.

Group Typical2 (fig. 15): This group differs from Group Typical1 with a median value of *MaxF* equal to 0.3 which indicates a relatively higher diversity at MS.

Group Typical3 (fig. 16): The features of group Typical3 indicate a relatively high frequential diversity and a relatively high spatial diversity at BS and MS. For groups Typical2 and Typical3, the street canyon effect is no more dominant as it was for group Typical1. The partitioning of MIMO points could be refined by dividing both groups into two sub-groups, one with a high street canyon effect and one with an almost uniform distribution of the MS-clusters around the mobile.

V. PARAMETER CORRELATION DISCUSSION

In this section we introduce the correlation between the different global parameters. In order to continue the comparison with the SCM model we added a new global parameter: the shadowing factor (*SF*). The shadowing factor is defined by (3):

$$SF\,(dB) = Ploss + Pr - Pe \qquad (3)$$

with
Pe: transmitted power
Pr: received wideband power averaged on 15 λ
Ploss: linear regression of the measured path loss

The path loss linear regression was processed on an extended set of measurement data (3000 instead of 804) (fig. 12). The histogram of *SF* is plotted in fig. 13. The standard deviation of *SF* is equal to 5.7 and is slightly lower than the standard deviation in the SCM urban macrocell model (8 dB).

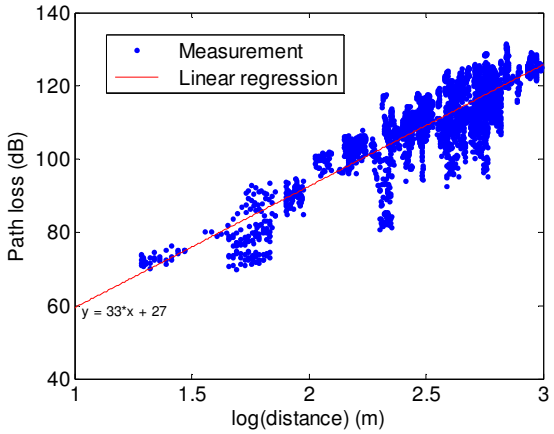

Figure 12: Shadowing factor estimation

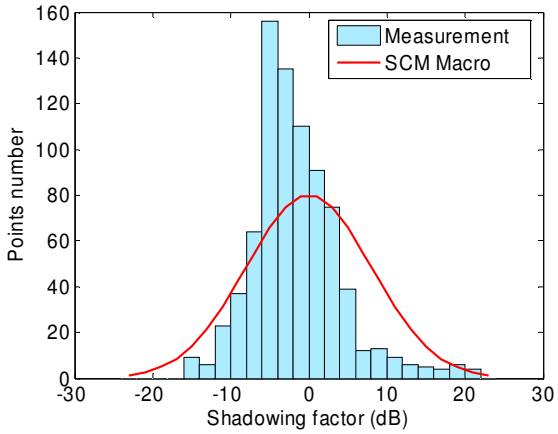

Figure 13: Histogram of SF

Table 2 sums up the global parameter correlation coefficients. The top right part contains correlation coefficients that were processed for all groups (typical and atypical). The bottom left part contains correlation coefficients that were only processed on the typical groups. The most significant difference concerns the correlation between AS and DS (0.21 with all groups, 0.6 with typical groups). This difference highlights the impact of the selected set of measurement data. A reduction of only 20 % of the total amount of data can significantly modify the correlation. It can partially explain divergent results found in the literature about the AS/DS correlation [19, 30, 31, 38]. Global parameters are slightly correlated with *Dist* or *MS-Azi*. The most correlated parameter with the distance is *AS* (-0.37). The correlation *ScF/MS-Azi* confirms the trend pointed out in groups Typical1 and LowAS: the street canyon effect is emphasized when *MS-Azi* decreases. Finally, the correlations DS/AS, DS/SF, AS/SF calculated on typical groups are close to those given by the SCM urban macro model. (AS/DS=0.5, SF/AS=-0.6, SF/DS=-0.6)

	Dist.	Az. MS	DS	BS-AS	Max fact.	SC fact.	Sh. Fact.
Dist.	1.00	-0.28	0.16	-0.55	0.19	0.28	0.16
Az. MS	-0.20	1.00	-0.02	0.32	-0.46	-0.60	-0.48
DS	0.03	0.03	1.00	0.21	-0.39	0.10	-0.32
BS-AS	-0.37	0.14	0.60	1.00	-0.46	-0.21	-0.40
Max Factor	0.09	-0.37	-0.45	-0.38	1.00	0.46	0.51
SC Factor	0.18	-0.53	0.00	0.02	0.46	1.00	-0.11
Sh. Factor	0.23	-0.32	-0.19	-0.37	0.33	-0.10	1.00

Table 2: Global parameter correlation

VI. Conclusion

In this paper, we have presented a method to create link-level propagation channel models from measurement data. This method was applied to measurements in macrocell environments at 2 GHz and we show that in 80 % of cases, the large variety of propagation channels could be represented by 3 typical files. Due to the conical ambiguity of the angle estimation method, the selected propagation channels do not properly model the elevation and azimuth at MS. Furthermore no information concerning the polarization is included. As a result, future work will focus on the analysis of the MS-DoAs and the polarization diversity. A measurement campaign using a bi-polar planar antenna array at MS is currently being processed. The results issuing from this campaign will complete the propagation channel models proposed in this paper.

VII. References

[1] D. Gesbert, M. Shafi, S. Da-shan, P. J. Smith, and A. Naguib, "From theory to practice: an overview of MIMO space-time coded wireless systems," *IEEE Journal on Selected Areas in Communications*, vol. 21, pp. 281, 2003.

[2] A. Goldsmith, S. A. Jafar, N. Jindal, and S. Vishwanath, "Capacity limits of MIMO channels," *IEEE Journal on Selected Areas in Communications*, vol. 21, pp. 684, 2003.

[3] K. Yu and B. Ottersten, "Models for MIMO propagation channels: a review," *Wireless Communications and Mobile Computing*, vol. 2, pp. 653, 2002.

[4] A. F. Molisch, "Effect of far scatterer clusters in MIMO outdoor channel models," presented at Vehicular Technology Conference (VTC 2003-Spring), 2003.

[5] J. P. Kermoal, L. Schumacher, K. I. Pedersen, P. E. Mogensen, and F. Frederiksen, "A stochastic MIMO radio channel model with experimental validation," *IEEE Journal on Selected Areas in Communications*, vol. 20, pp. 1211, 2002.

[6] K. I. Pedersen, J. B. Andersen, J. P. Kermoal, and P. Mogensen, "A stochastic multiple-input-multiple-output radio channel model for evaluation of space-time coding algorithms," presented at Vehicular Technology Conference (VTC-Fall 2000), 2000.

[7] L. Correia, *Mobile Broadband Multimedia Networks: Techniques, Models and tools for 4G*: Academic Press, 2006.

[8] R. B. Ertel, P. Cardieri, K. W. Sowerby, T. S. Rappaport, and J. H. Reed, "Overview of spatial channel models for antenna array communication systems," *IEEE Personal Communications*, vol. 5, pp. 10, 1998.

[9] H. Hofstetter, A. F. Molisch, and N. Czink, "A twin-cluster MIMO channel Model," presented at EuCAP, Nice, 2006.
[10] "Spatial channel model for Multiple Input Multiple Output (MIMO) simulations," 3GPP TR 25.996 V6.1.0, 2003.
[11] X. Hao, D. Chizhik, H. Huang, and R. Valenzuela, "A generalized space-time multiple-input multiple-output (MIMO) channel model," *IEEE Transactions on Wireless Communications*, vol. 3, pp. 966, 2004.
[12] F. A. Agelet, A. Formella, J. M. H. Rabanos, F. I. d. Vicente, and F. P. Fontan, "Efficient Ray-Tracing Acceleration Techniques for Radio Propagation Modeling," *IEEE Transactions on Vehicular Technology*, 2000.
[13] T. Fugen, J. Maurer, T. Kayser, and W. Wiesbeck, "Verification of 3D Ray-tracing with Non-Directional and Directional Measurements in Urban Macrocellular Environments," presented at VTC 2006, Melbourne, 2006.
[14] M. A. Jensen and J. W. Wallace, "A review of antennas and propagation for MIMO wireless communications", *IEEE Transactions on Antennas and Propagation*, vol. 52, pp. 2810, 2004.
[15] M. Steinbauer, A. F. Molisch, and E. Bonek, "The double-directional radio channel," *IEEE Antennas and Propagation Magazine*, vol. 43, pp. 51, 2001.
[16] 3GPP, "Spatial Channel model for MIMO Simulations," http://www.3GPP.org, vol. TR 25.996 V6.1.0., 2003.
[17] 3GPP, "Physical layer aspects for evolved Universal Terrestrial Radio Access (UTRA)," http://www.3GPP.org, vol. TR 25.814 V7.0.0, 2006.
[18] J. M. Conrat and P.Pajusco, "A Versatile Propagation Channel Simulator for MIMO Link Level Simulation," presented at COST 273 TD(04)120, Paris, 2003.
[19] P. Laspougeas, P. Pajusco, and J. C. Bic, "Radio propagation in urban small cells environment at 2 GHz: experimental spatio-temporal characterization and spatial wideband channel model," presented at Vehicular Technology Conference (VTC 2000), Boston, 2000.
[20] P. Laspougeas, P. Pajusco, and J. C. Bic, "Spatial radio channel model for UMTS in urban small cells area," presented at European Conference on Wireless Technology, Paris, 2000.
[21] J. M. Conrat and P. Pajusco, "Clusterization of the MIMO Propagation Channel in urban macrocells at 2 GHz," presented at European Conference on Wireless Technology (ECWT), Paris, 2005.
[22] A. Kuchar, J. P. Rossi, and E. Bonek, "Directional macro-cell channel characterization from urban measurements," *IEEE Transactions on Antennas and Propagation*, vol. 48, pp. 137, 2000.
[23] J. Laurila, K. Kalliola, M. Toeltsch, K. Hugl, P. Vainikainen, and E. Bonek, "Wideband 3D characterization of mobile radio channels in urban environment," *IEEE Transactions on Antennas and Propagation*, vol. 50, pp. 233, 2002.
[24] L. Vuokko, K. Sulonen, and P. Vainikainen, "Analysis of propagation mechanisms based on direction-of-arrival measurements in urban environments at 2 GHz frequency range," presented at Antennas and Propagation International Symposium, 2002.
[25] K. Kalliola, H. Laitinen, P. Vainikainen, M. Toeltsch, J. Laurila, and E. Bonek, "3-D double-directional radio channel characterization for urban macrocellular applications," *IEEE Transactions on Antennas and Propagation*, vol. 51, pp. 3122, 2003.
[26] M. Toeltsch, J. Laurila, K. Kalliola, A. F. Molisch, P. Vainikainen, and E. Bonek, "Statistical characterization of urban spatial radio channels," *IEEE Journal on Selected Areas in Communications*, vol. 20, pp. 539, 2002.
[27] U. Martin, "Spatio-temporal radio channel characteristics in urban macrocells," *IEE Proceedings - Radar, Sonar and Navigation*, vol. 145, pp. 42, 1998.
[28] M. Pettersen, P. H. Lehne, J. Noll, O. Rostbakken, E. Antonsen, and R. Eckhoff, "Characterisation of the directional wideband radio channel in urban and suburban areas," presented at Vehicular Technology Conference (VTC-Fall 1999), 1999.
[29] M. Larsson, "Spatio-temporal channel measurements at 1800 MHz for adaptive antennas," presented at Vehicular Technology Conference (VTC 1999), 1999.
[30] M. Nilsson, B. Lindmark, M. Ahlberg, M. Larsson, and C. Beckman, "Measurements of the spatio-temporal polarization characteristics of a radio channel at 1800 MHz," presented at Vehicular Technology Conference (VTC 1999), 1999.
[31] K. I. Pedersen, P. E. Mogensen, and B. H. Fleury, "A stochastic model of the temporal and azimuthal dispersion seen at the base station in outdoor propagation environments," *IEEE Transactions on Vehicular Technology*, vol. 49, pp. 437, 2000.
[32] B. Allen, J. Webber, P. Karlsson, and M. Beach, "UMTS spatio-temporal propagation trial results," presented at IEE International Conference on Antenna and Propagation, Manchester, 2001.
[33] S. E. Foo, M. A. Beach, P. Karlsson, P. Eneroth, B. Lindmark, and J. Johansson, "Spatio-temporal investigation of UTRA FDD channels," presented at International Conference on 3G Mobile Communication Technologies, 2002.
[34] S. E. Foo, C. M. Tan, and M. A. Beach, "Spatial temporal characterization of UTRA FDD channels at the user equipment," presented at Vehicular Technology Conference (VTC 2003-Spring), 2003.
[35] L. Vuokko, V.-M. Kolmonen, J. Kivinen, and P. Vainikainen, "Results from 5.3 GHz MIMO measurement campaign," presented at COST 273 TD(04)193, Duisburg, 2004.
[36] U. Trautwein, M. Landmann, G. Sommerkorn, and R. Thomä, "Measurement and Analysis of MIMO Channels in Public Access Scenarios at 5.2 GHz," presented at International Symposium on Wireless Personal Communications, Aalborg, 2005.
[37] J. Medbo, M. Riback, H. Asplund, and J.-E. Berg, "MIMO Channel Characteristics in a Small Macrocell measured at 5.25 GHz and 200 MHz Bandwidth," presented at VTC-Fall 2005, Dallas, 2005.
[38] A. Algans, K. I. Pedersen, and P. E. Mogensen, "Experimental analysis of the joint statistical properties of azimuth spread, delay spread, and shadow fading," *IEEE Journal on Selected Areas in Communications*, vol. 20, pp. 523, 2002.

	All groups			Atypical			Typical		
	10%	50%	90%	High DS	High AS	Low BS-AS	Type 1	Type 2	Type 3
Occurrence %	-	-	-	5%	5%	10%	30%	30%	20%
Distance (m)	194	360	598	327	33	530	382	411	316
MS-Angle (°)	6.7	40.3	78	30	47	5	32	45	54
DS (ns)	99	227	421	540	110	123	159	195	319
BS-AS (°)	1.13	8.2	18.4	7.7	24	0.7	3.62	6.6	15
MaxR	0.13	0.32	0.73	0.2	0.24	0.7	0.7	0.29	0.23
ScR	0.09	0.46	0.91	0.53	0.18	0.9	0.8	0.37	0.4

Table 2 : Statistics of global parameters

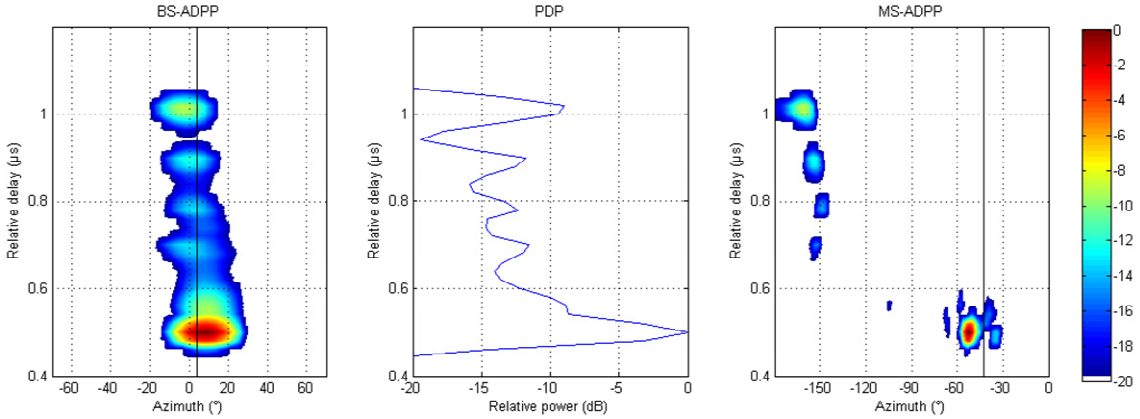

Figure 14: Example for Typical1 profiles: *AS*=3.9°, *DS*=175 ns, *MaxF*= 0.69, *ScF* = 0.13

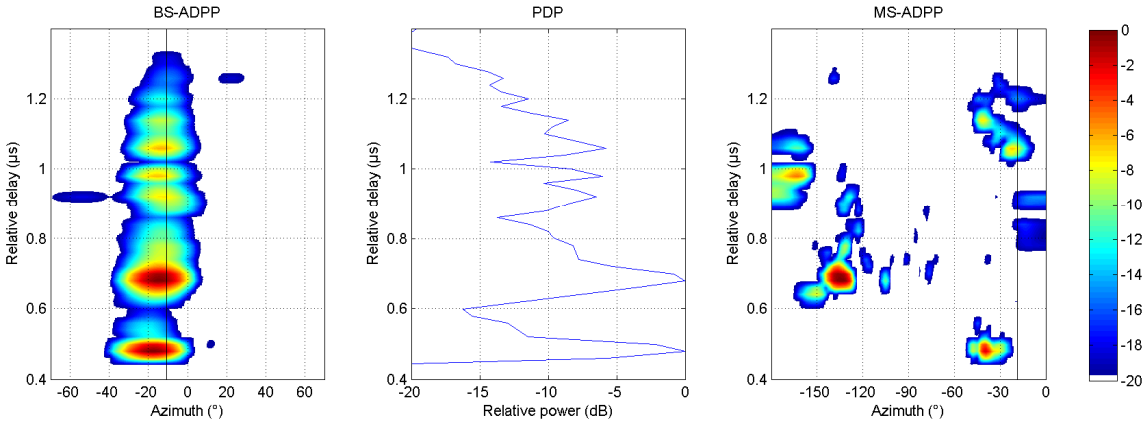

Figure 15: Example for Typical2 profiles: *AS*=4.6°, *DS*=244 ns, *MaxF*=0.27, *ScF*=0.22

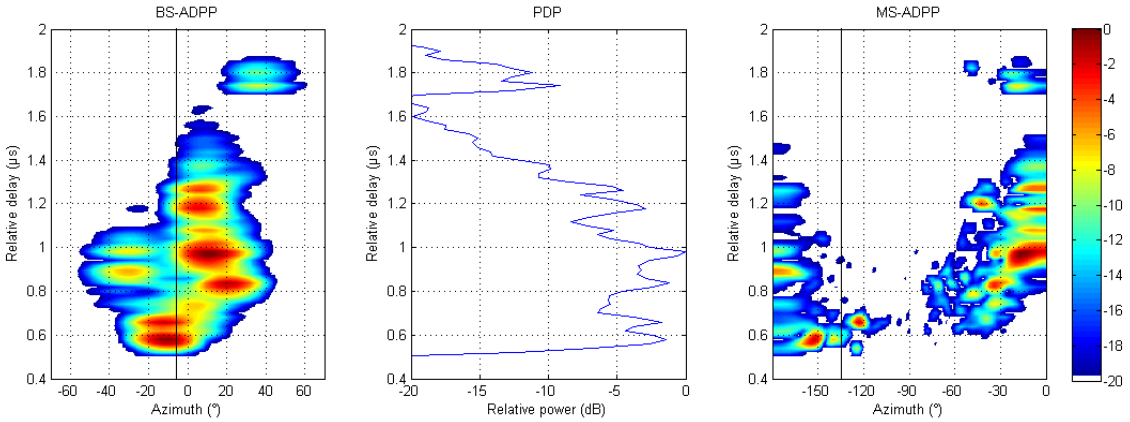

Figure 16: Example for Typical3 profiles: *AS*=16.1°, *DS*=303 ns, *MaxF*=0.11, *ScF*=0.41

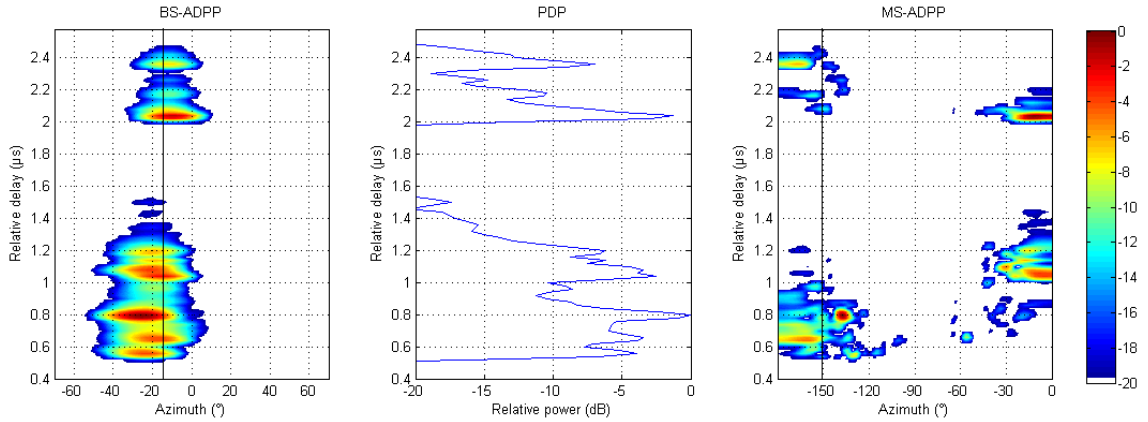

Figure 17: Example for HighDS profiles, *AS*=5.8°, *DS*= 550 ns, *MaxF*= 0.1400, *ScF*=0.5

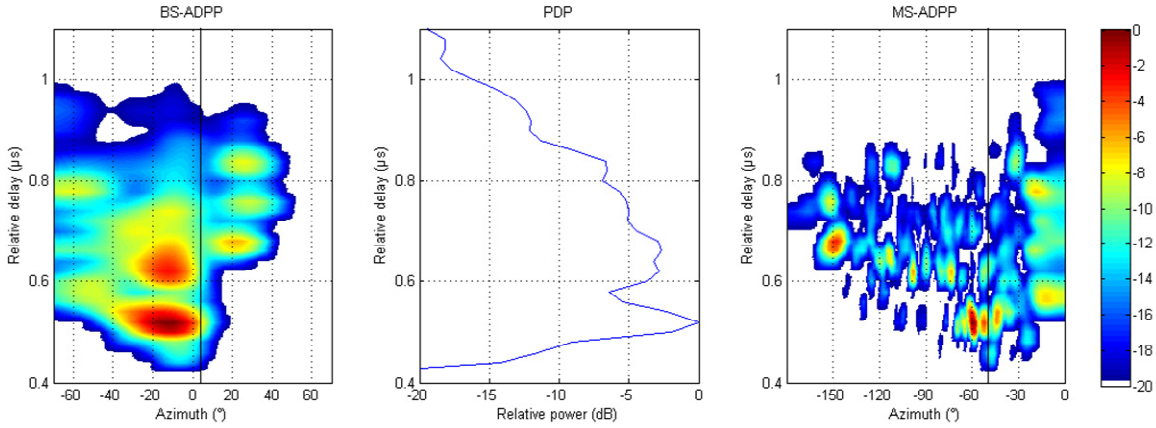

Figure 18: Example for HighAS profiles, *AS*=22.9°, *DS*=111 ns, *MaxF*=0.14, *ScF*=0.11

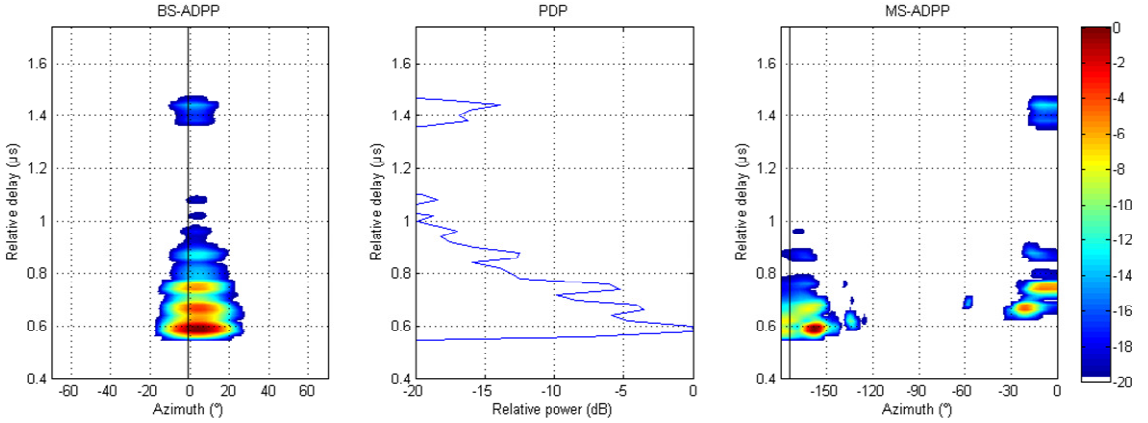

Figure 19: Example for LowAS profiles, *AS*=0.5°, *DS*=169 ns, *MaxF*=0.37, *ScF*=0.92